A High Torque Density MEMS Magnetic Induction Machine

H. Köşer* (*hurkoser@mit.edu*), F. Cros**, M. G. Allen**, and J. H. Lang*

*Microsystems Technology Laboratories, Laboratory for Electromagnetic and Electronic Systems, Massachusetts Institute of Technology, Cambridge, MA 02139, USA

**Microelectronics Research Center, Georgia Institute of Technology, Atlanta, GA 30332, USA

ABSTRACT

Most micro-scale electric and magnetic machines developed over the last decade lack the torque and power density to support many practical applications. The micro-scale magnetic induction machine reported here attempts to transcend this practicality barrier by offering a torque density exceeding 15% of that exhibited by macro-scale magnetic machines. The experimental magnetic induction motor described here is a two-phase planar motor fabricated from electroplated NiFe and Cu. It is approximately 8 mm in diameter, including end-turns, and 2 mm thick. Its rotor is suspended above its stator on tethers, or springs, so as to permit accurate torque measurements. The rotor-stator air gap is approximately 5 μm. With a balanced phase excitation of 2.5 A peak, the motor produces a torque of 1.2 μNm. Therefore, if the phase excitation is raised to 13 A peak, which has been achieved experimentally, a torque of 32.4 μNm is expected, corresponding to a torque density over 322 Nm/m^3.

Keywords: Power MEMS, Induction Machine, Electroplating.

1 INTRODUCTION

This paper describes a high-torque-density micro-scale magnetic induction motor. The device is a planar two-phase motor fabricated from electroplated NiFe and Cu; NiFe is used for the magnetic core and Cu is used for the conducting windings. It is designed for use within micro turbomachinery [1]. This paper begins with a review of the modeling and design of the motor. Next, it describes the fabrication of the motor in detail. Finally, it presents the initial measurements of motor torque and winding ampacity.

2 GEOMETRY & ANALYSIS

For fabrication simplicity and compatibility with micro turbomachinery, the induction machine studied here is planar, as shown in Figure 1. The rotor stands just above the stator, supported by air bearings [1]. The stator carries two phases, each with one conductor per slot. Four slots are allocated per pole pair, and the phases are displaced from each other by one slot so as to be magnetically orthogonal.

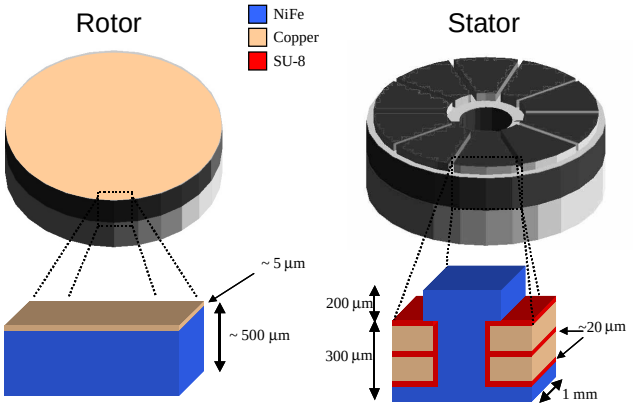

Figure 1: Rotor and stator of a typical MEMS magnetic induction machine (end-turns are not shown).

The axial symmetry of the magnetic induction machine simplifies its modeling by allowing a mapping of each circular cross-section at a given radius into Cartesian coordinates, as shown in Figure 2. Modeling then proceeds by developing a 2D boundary layer solution of Maxwell's Equations for the rotor, and a magnetic circuit for the stator.

Figure 3 shows a cross-section of the rotor. Magnetic fields within the rotor obey the equations of magnetic diffusion in uniform moving materials. Following [2], they are determined from these equations assuming that they vanish on the upper-most air surface in Figure 3, and that they are expanded in a Fourier Series at the surface of the stator. A separate determination is carried out for each mode in the expansion.

The stator is spatially non-uniform, with features such as poles, slots, and windings. Hence, the stator is most easily modeled using magnetic circuits. Figure 4 shows the magnetic circuit used here. The reluctances in the circuit are based on the geometry and permability of the NiFe stator core, as fabricated.

To complete the model of the magnetic induction machine, the magnetic circuit model of the stator must be joined to the distributed model of the rotor at the in-

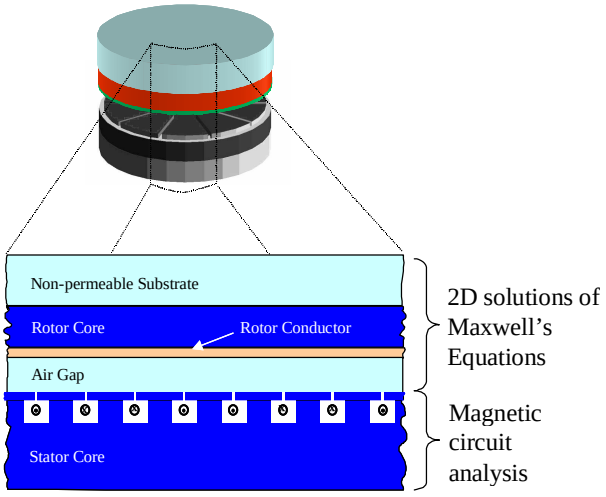

Figure 2: The modeling approach.

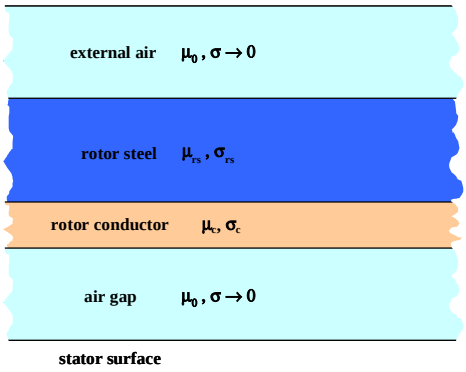

Figure 3: The geometry and properties of the multilayered rotor. The top air layer extends to infinity.

terface between the air gap and the stator. To do so, the lumped tangential magnetic field and the lumped normal magnetic flux density (Φ_1-Φ_4) in the stator circuit are distributed over their respective regions. The resulting distributed fields are expanded in Fourier Series along the interface. These series are then coupled mode-by-mode to the rotor model, yielding a complete model of the machine which can be analyzed for all magnetic fields within the machine. Having determined the fields within the machine, it is then possible to determine the losses in the conductors of the machine, and the torque and axial force which act on the rotor at a given radius. Here, the torque and force are calculated using the Maxwell Stress Tensor [2]. Finally, these quantities are integrated over the machine radius to obtain their totals.

The analysis of the coupled rotor and stator models is implemented in a MATLAB/C program. The program takes geometry and material properties as inputs,

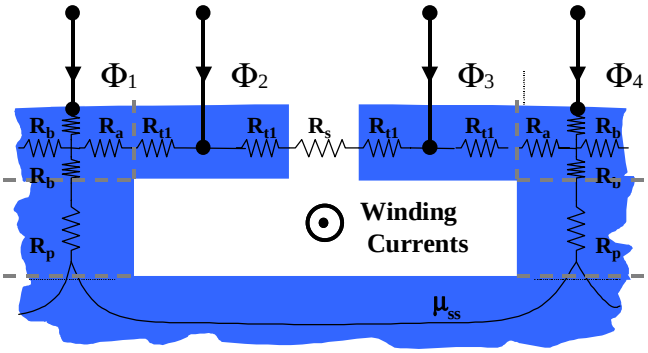

Figure 4: Magnetic circuit of the stator.

and provides rotor torque and axial force, and conductor losses as outputs [4]. The accuracy of this program has been verified through comparison with magnetic finite-element analysis, and its worst-case errors are typically less than a few percent [4].

Using the program a first-generation motor has been designed. Its geometry and dimensions are shown in Figure 1. This motor has been fabricated as discussed in Section 3, and tested as discussed in Section 4.

3 FABRICATION

The primary challenge in fabricating a micromachined magnetic induction machine is interspersing and stacking thick multi-layer conductors and large volumes of magnetic material to form its stator. To meet this challenge, we have used a Micro-Molding, and Electroplating (MIME) process. In order to fabricate tall electroplated structures, thick photosensitive SU-8 polymer is used for the molds. This negative photosensitive epoxy permits the fabrication of high aspect ratio molds [3]. Using such molds, the fabrication of a two-coil stator occurs in three distinct phases, as shown Figure 5: (a) fabrication of the first level of Cu windings and NiFe core, (b) fabrication of the second level of Cu winding and NiFe core and (c) fabrication of the NiFe pole faces.

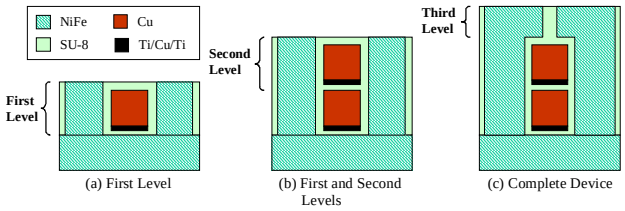

Figure 5: General fabrication process for the two-winding stator.

The fabrication process starts with a 1 mm thick NiFe substrate which possesses the appropriate magnetic properties for machine operation. Next, the MIME

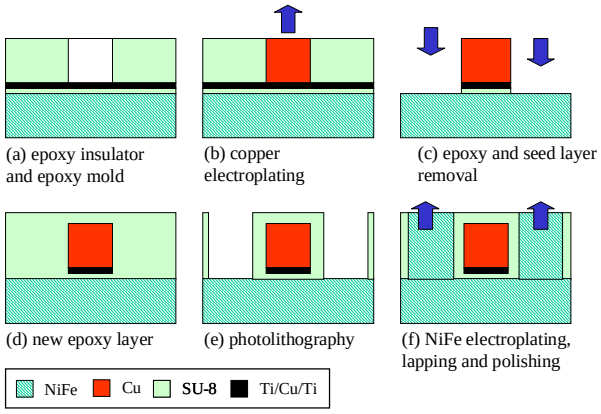

Figure 6: Fabrication process for the first stator level.

process is applied to fabricate the first-level winding and core. A 25 μm insulation layer of epoxy is then spun, cross-linked and cured on top of the substrate. The epoxy is patterned and Cu is electroplated in order to form a winding (Fig 6 (a),(b)). The epoxy mold around the windings as well as the insulation layer at the foot of the Cu structure is removed by plasma etch (Fig 6 (c)). A thick layer of epoxy is then spun on top of the first winding (Fig 6 (d)). The epoxy permits planarization of the surface above the pre-existing Cu windings. Later, the epoxy is patterned by conventional photolithography in order to create a mold for the NiFe poles (Fig 6 (e)). At this point, the Cu winding is completely embedded in the epoxy. Next, NiFe is electroplated in the cavities in the epoxy mold. Finally, the upper surface of the structure is lapped and polished (Fig 6 (f)). In order to form the full stator shown in Figure 5, this MIME process is repeated for the second level, and again in a simpler manner for the third level.

Figure 7 shows a SEM of the two windings surrounding the NiFe poles. Here, the epoxy has been partially

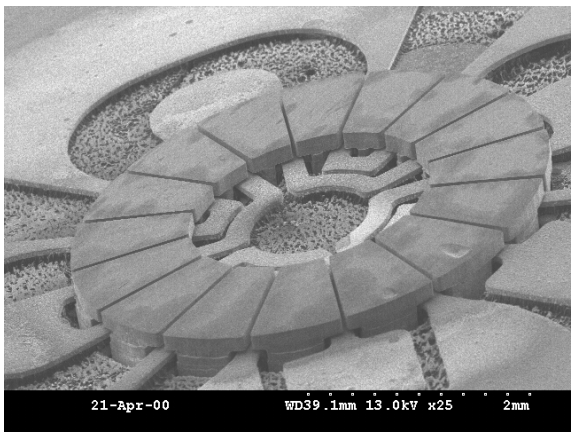

Figure 7: Finished stator.

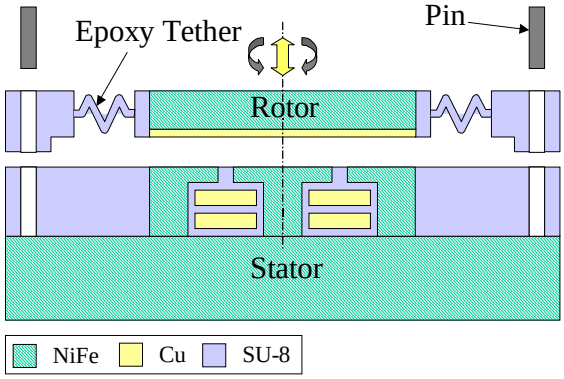

Figure 8: Schematic cross-section of the tethered motor

removed so that the winding structure may be clearly observed. The total height of the device, excluding the substrate, is approximately 500 μm.

The fabrication of the rotor is considerably simpler since it consists only of a NiFe disk with a thin layer of electroplated Cu at the airgap. For the machine reported here, the rotors are encapsulated in SU-8 epoxy and suspended above the stator with SU-8 epoxy tethers. A package was fabricated in order to accommodate the integration of the rotor and the stator. Alignment holes on both dies allow control of the relative orientation of the rotor and the stator using locator pins, as shown in Figure 8.

4 EXPERIMENTS

Two-phase power electronics have been built to deliver a balanced excitation (up to 20 A and 100 kHz) in quadrature through the two windings in the stator. A torque-reversal switch which swaps the phase excitations has been implemented to switch the direction of the applied torque, at frequencies far lower than the input electrical frequency. By periodically reversing the torque, the mechanical resonance of the rotor and tethers can be excited. The response of this resonance as a function of torque reversal frequency can be used to determine the rotor torque.

A typical tether resonance response is shown in Figure 9. The figure displays the peak azimuthal deflection of the rotor at its outer radius of 2 mm as a function of the mechanical torque reversal frequency. For the data shown in Figure 9, the peak stator phase current amplitude is 2.5 A, and its electrical frequency is 30 kHz. In addition, the figure shows a solid second-order resonance curve that is fit to the data. This curve is based on an inertia calculated from the rotor dimensions and density. It is also based on a combination of torque amplitude, tether stiffness and viscous damping coefficient that yields the best fit to the data. In this way, torque is extracted from the data.

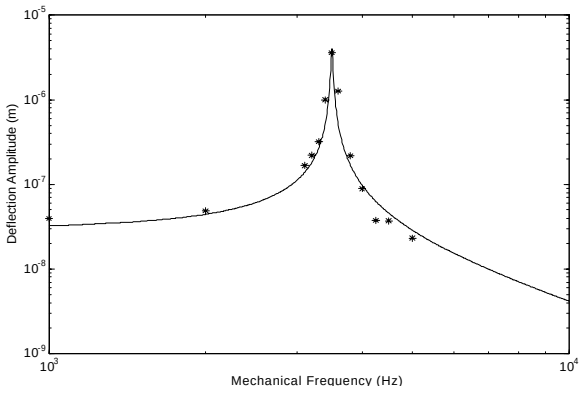

Figure 9: Mechanical resonance of the tethered rotor.

The process of torque extraction is repeated for several experiments, over which the amplitude of the stator currents remains constant as the electrical frequency varies. The extracted torque is displayed as a function of electrical stator frequency in Figure 10. Additionally,

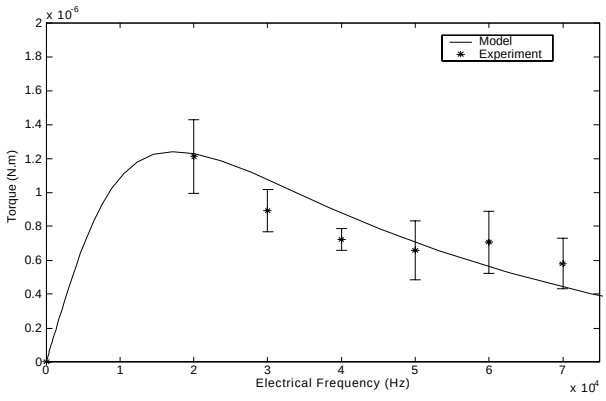

Figure 10: Model and experimental torque as a function of electrical frequency.

the figure shows a torque prediction from the analysis program described in Section 2. The quality of the fit validates the model described in Section 2, and detailed in [4].

In separate experiments, a stator was excited safely and continuously with peak currents up to 13 A without damage. This corresponds to a current density of more than 10^9 A/m^2, which greatly exceeds the current density in macro-scale magnetic machines. Further, this current level does not cause magnetic saturation. Therefore, we expect that the machine is capable of producing up to $(13/2.5)^2 \times 1.2$ μNm, or 32.4 μNm; the associated torque density is about 322 Nm/m^3. This is about 15% of the torque density produced by a macro-scale induction motor. Unfortunately, this torque could not be demonstrated because the epoxy tethers were incapable of supporting the corresponding axial force.

5 SUMMARY AND CONCLUSIONS

This paper presents the design, fabrication and testing of a micro-scale magnetic induction motor. Fabrication is based on the electroplating of NiFe cores and Cu conductors, with SU-8 epoxy serving as both the molds and insulators. The experimental motor has a 4 mm radius, including end-turns, and a 2 mm axial length. When excited with 2.5 A stator currents it produces a torque of 1.2 μNm. This measured torque compares well to the modeled torque, thereby validating the models reported in [4].

It is known that the experimental motor can operate safely, and in the absence of magnetic saturation, with 13 A peak stator currents. In this case, the motor would produce a torque of 32.4 μNm, thereby achieving a torque density of 322 Nm/m^3. This is comparable to what can be achieved by common macro-scale magnetic motors.

6 ACKNOWLEDGMENTS

This work is supported by ARO grant DAAG55-98-1-0292, Dr. Thomas L. Doligalski, scientific officer. The authors wish to thank Professor Denny Freeman at MIT for use of the microvision system on which the deflection/torque measurements were made.

REFERENCES

[1] Epstein, A. H., et al., *"Power MEMS and Microengines"*, IEEE Conf. Solid State and Actuators, June 1997

[2] Melcher, J. R., *"Continuum Electromechanics"*, Table 6.5.1, pp. 6.12, MIT Press, 198*1*

[3] Despont, M, et. al., *"High-Aspect-Ratio, Ultrathick, Negative-Tone Near-UV Photoresist for MEMS"*, Proc. of IEEE 10$^{\text{th}}$ Annual International Workshop on MEMS, Nagoya, Japan, pp. 518-522, 1997.

[4] Köşer, H., and Lang, J. H., *"Modeling A High Power Density MEMS Magnetic Induction Machine"*, Proc. of International Conf. on Modeling and Simulation of Microsystems, Hilton Head, SC, USA, pp. 286-289, 2001.